1
Optical Refrigeration in Solids: Fundamentals and Overview

Richard I. Epstein and Mansoor Sheik-Bahae

1.1
Basic Concepts

Optical refrigeration, or the cooling of solids with near-monochromatic light, is a discipline that was anticipated almost 80 years ago, decades before the invention of the laser. In 1929, the German physicist Peter Pringsheim (Figure 1.1) proposed the cooling of solids by fluorescence upconversion [3]. Because of the great advances that have been made in the use of lasers to cool and trap dilute gases of atoms and ions to extremely low temperatures, the term "laser cooling" is most often used in reference to this area of science. This is quite justified given its spectacular achievements, such as the creation of Bose–Einstein condensates and many related phenomena [1, 2]. Nevertheless, optical refrigeration is itself a rapidly growing field; one that offers insights into the interaction of light with condensed matter, and has the potential to provide the basis for new types of cryogenic refrigeration. In the solid phase, thermal energy is largely contained in the vibrational modes of the lattice. In the laser cooling of solids, light quanta in the red tail of the absorption spectrum are absorbed from a monochromatic source, and then spontaneous emission of more energetic (blue-shifted) photons occurs. The extra energy is extracted from lattice phonons, the quanta of vibrational energy that are generated from heat. The removal of these phonons is therefore equivalent to cooling the solid. This process has also been termed "anti-Stokes fluorescence" and "luminescence upconversion" cooling.

Laser cooling of solids can be exploited to achieve an all-solid-state cryocooler [4–6], as conceptually depicted in Figure 1.2. The advantages of compactness, no vibrations, no moving parts or fluids, high reliability, and no need for cryogenic fluids have motivated intensive research. Spaceborne infrared sensors are likely to be the first beneficiaries, with other applications requiring compact cryocooling reaping the benefits as the technology progresses. A study by Ball Aerospace Corporation [7] shows that in low-power spaceborne operations, ytterbium-based optical refrigeration could outperform conventional thermoelectric and mechanical coolers in the temperature range 80 – 170 K. Efficient, compact semiconductor lasers can pump optical refrigerators. In many potential applications, the requirements

Optical Refrigeration. Science and Applications of Laser Cooling of Solids.
Edited by Richard Epstein and Mansoor Sheik-Bahae

ISBN: 978-3-527-40876-4

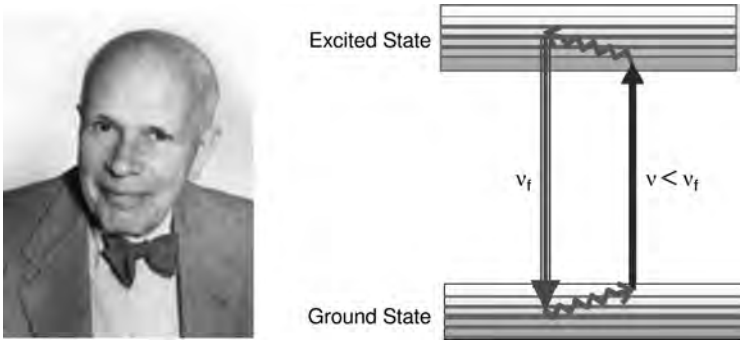

Figure 1.1 In 1929, Peter Pringsheim suggested that solids could cool through anti-Stokes fluorescence, in which a substance absorbs a photon and then emits one of greater energy. The energy diagram on the *right* shows one way in which this could occur. An atom with two broad levels is embedded in a transparent solid. The light source of frequency $h\nu$ excites atoms near the top of the ground state level to the bottom of the excited state. Radiative decays occurring after thermalization emit photons with average energy $h\nu_f > h\nu$.

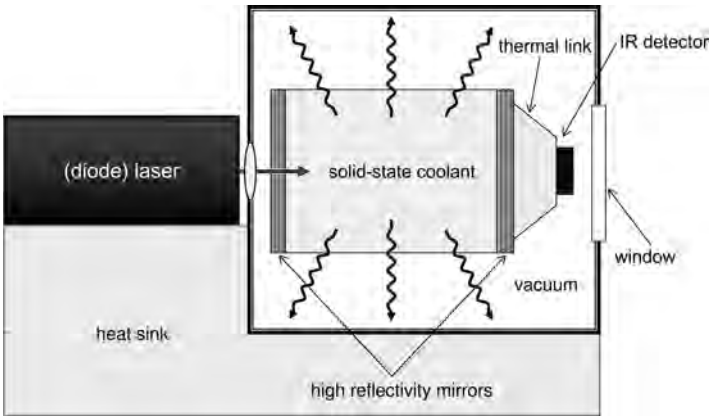

Figure 1.2 Schematic of an optical refrigeration system. Pump light is efficiently generated by a semiconductor diode laser. The laser light enters the cooler through a pinhole in one mirror and is trapped by the mirrors until it is absorbed. Isotropic fluorescence escapes the cooler element and is absorbed by the vacuum casing. A sensor or some other load is connected in the *shadow region* of the second mirror. Figure 1.2 has been reproduced from [6].

on the pump lasers are not very restrictive. The spectral width of the pump light has to be narrow compared to the thermal spread of the fluorescence. A multimode fiber-coupled laser with a spectral width of several nanometers would be adequate. In an optical refrigerator, the cooling power is of the order 1% of the pump laser power. Only modest lasers are adequate for microcooling applications with a heat lift of mW. For larger heat lifts, correspondingly more powerful lasers are needed. In all cooling applications, the cooling element has to be connected to the device being cooled, the *load*, by a thermal link; see Figure 1.2. This link siphons heat

from the load while preventing the waste fluorescence from hitting the load and heating it. See also Chapter 5 by Mills and Buchwald for further discussion on the practical implementation of all-solid-state cryocoolers in rare-earth-doped solids.

Another potential application of laser cooling of solids is to eliminate heat production in high-power lasers. Even though laser emission is always accompanied by heat production, Bowman [8, 9] realized that in some laser materials, the pump wavelength can be adjusted so that the spontaneous anti-Stokes fluorescence cooling compensates for the laser heating. Such a thermally balanced laser would not suffer from thermal defocusing or heat damage.

The process of optical refrigeration can occur only in special high-purity materials (see Section 1.3) that have appropriately spaced energy levels and emit light with a high quantum efficiency. To date, optical refrigeration research has been confined to glasses and crystals doped with rare-earth elements and direct-band semiconductors such as gallium arsenide. Laser cooling of rare-earth-doped solids has been successfully demonstrated, while observations of net cooling in semiconductors have remained elusive. Figure 1.1 schematically depicts the optical refrigeration processes for a two-level system with vibrationally broadened ground- and excited-state manifolds. Photons from a low-entropy light source (i.e. a laser) with energy $h\nu$ excite atoms from the top of the ground state to the bottom of the excited state. The excited atoms reach quasi-equilibrium with the lattice by absorbing phonons. Spontaneous emission (fluorescence) follows, with a mean photon energy $h\nu_f$ that is higher than that of the absorbed photon. This process has also been called anti-Stokes fluorescence. There were initial concerns that the second law of thermodynamics might be violated until Landau clarified the issue in 1946 by assigning an entropy to the radiation [10].

In the aforementioned simple model, the interaction rate between electrons and phonons within each manifold is assumed to be far faster than the spontaneous emission rate, which is valid for a broad range of materials and temperatures. The cooling efficiency or fractional cooling energy for each photon absorbed is

$$\eta_c = \frac{h\nu_f - h\nu}{h\nu} = \frac{\lambda}{\lambda_f} - 1 \,, \tag{1.1a}$$

where $\lambda = c/\nu$ is the wavelength. The invention of the laser in 1960 prompted several unsuccessful attempts to observe laser cooling of solids [11–13]. In 1995, net cooling was first achieved by workers at Los Alamos National Laboratory [14]. Two technical challenges were addressed and overcome in these experiments. The Los Alamos researchers had to have a system in which (i) the vast majority of optical excitations recombine radiatively and (ii) there is a minimal amount of parasitic heating due to unwanted impurities. Both of these critical engineering issues are ignored in the idealized situation described by (1.1a), but are key to experimental success.

It is also important that spontaneously emitted photons escape the cooling material without being trapped and re-absorbed, which would effectively inhibit spontaneous emission [15, 16]. This is a critical issue for high-index semiconductors where total internal reflection can cause strong radiation trapping. In the absence

of radiation trapping, the fraction of atoms that decay to the ground state by the desired radiative process is known as the quantum efficiency, $\eta_q = W_{rad}/(W_{rad} + W_{nr})$, where W_{rad} and W_{nr} are radiative and nonradiative decay rates, respectively. Including a fluorescence escape efficiency η_e defines an external quantum efficiency (EQE), $\eta_{ext} = \eta_e W_{rad}/(\eta_e W_{rad} + W_{nr})$, which assumes the fluorescence is reabsorbed within the excitation volume (see Section 1.4). This describes the efficiency by which a photoexcited atom decays into an escaped fluorescence photon in free space. In a similar fashion, an absorption efficiency $\eta_{abs} = \alpha_r/(\alpha_r + \alpha_b)$ is defined to account for the fraction of pump laser photons that are engaged in cooling [6, 17]. Here α_r is the resonant absorption coefficient and α_b is the unwanted parasitic (background) absorption coefficient. As will be derived in Sections 1.2 and 1.4, the combination of all of these effects redefines the cooling efficiency as:

$$\eta_c = \eta_{ext}\eta_{abs}\frac{\lambda}{\lambda_f} - 1 \,, \tag{1.1b}$$

where the product $\eta_{ext}\eta_{abs}$ indicates the efficiency of converting an absorbed laser photon to an escaped fluorescence photon. Note that η_{abs} is frequency dependent and falls off rapidly below a photon energy $h\nu_f - k_B T$, where k_B is the Boltzmann constant and T is the lattice temperature. At pump photon energies of much more than $k_B T$ below $h\nu_f$, η_{abs} is too small to make $\eta_c > 0$ and laser cooling is unattainable. The above analysis defines the approximate condition needed for laser cooling [6, 17]:

$$\eta_{ext}\eta_{abs} > 1 - \frac{k_B T}{h\nu_f} \,. \tag{1.2}$$

This relation quantifies the required efficiencies: cooling a material from room temperature with a nominal energy gap (pump photon) of 1 eV from room temperature demands that $\eta_{ext}\eta_{abs} > 97\%$. Although suitable lasers were available in the early 1960s, more than three decades of progress in material growth were needed to satisfy this condition.

1.2 The Four-Level Model for Optical Refrigeration

Consider the four-level system of Figure 1.3 in which the ground-state manifold consist of two closely spaced levels of $|0\rangle$ and $|1\rangle$ with an energy separation of δE_g. The excited manifold consists of two states $|3\rangle$ and $|2\rangle$ with an energy separation δE_u. Laser excitation at $h\nu$ is tuned to be in resonance with the $|1\rangle$–$|2\rangle$ transition, as shown by the solid red arrow. The double-line arrows depict the spontaneous emission transitions from the upper level to the ground states with a rate of W_{rad}; this rate is assumed to be the same for all four transitions. The nonradiative decay rates (indicated by the dotted lines) are also assumed to be equal and given by W_{nr}. The population in each manifold reaches a quasi-thermal equilibrium via an

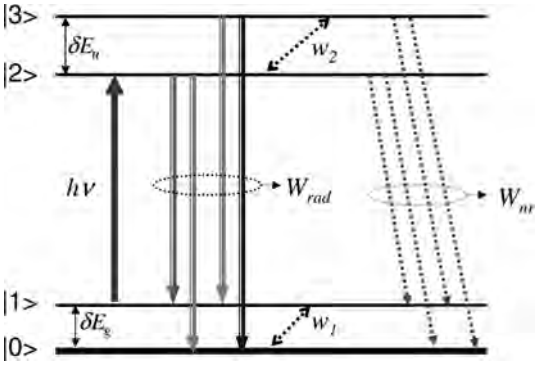

Figure 1.3 The four-level energy model for optical refrigeration consisting of two pairs of closely spaced levels: $|0\rangle$ and $|1\rangle$ in the ground state and $|2\rangle$ and $|3\rangle$ in the excited-state manifolds.

electron–phonon interaction rate given by w_1 and w_2 for lower and upper states, respectively.

The rate equations governing the density populations N_0, N_1, N_2, and N_3 are:

$$\frac{dN_1}{dt} = -\sigma_{12}\left(N_1 - \frac{g_1}{g_2}N_2\right)\frac{I}{h\nu} + \frac{R}{2}(N_2 + N_3) - w_1\left(N_1 - \frac{g_1}{g_0}N_0 e^{-\delta E_g/k_B T}\right), \tag{1.3a}$$

$$\frac{dN_2}{dt} = \sigma_{12}\left(N_1 - \frac{g_1}{g_2}N_2\right)\frac{I}{h\nu} - RN_2 + w_2\left(N_3 - \frac{g_3}{g_2}N_2 e^{-\delta E_u/k_B T}\right), \tag{1.3b}$$

$$\frac{dN_3}{dt} = -RN_3 - w_2\left(N_3 - \frac{g_3}{g_2}N_2 e^{-\delta E_u/k_B T}\right), \tag{1.3c}$$

$$N_0 + N_1 + N_2 + N_3 = N_t, \tag{1.3d}$$

where $R = 2W_{rad} + 2W_{nr}$ is the total upper state decay rate, σ_{12} is the absorption cross-section associated with the $|1\rangle$–$|2\rangle$ transition, I is the incident laser irradiance, and the g_i terms represent degeneracy factors for each level. The weighting factor in the electron–phonon interaction terms (w_1 and w_2) maintains the Boltzmann distribution among each manifold at quasi-equilibrium. The net power density deposited in the system is the difference between the absorbed and the radiated contributions:

$$P_{net} = \sigma_{12}N_1 1 - \frac{g_1 N_2}{g_2 N_1} I - W_{rad}[N_2(E_{21} + E_{20}) + N_3(E_{31} + E_{30})] + \alpha_b I, \tag{1.4}$$

where the first term is the laser excitation ($|1\rangle$–$|2\rangle$ transition) and the second term includes the spontaneous emission terms from levels $|2\rangle$ and $|3\rangle$ with their respective photon energies. We have also included a term that represents the parasitic absorption of the pump laser with an absorption coefficient of α_b. It is straightforward to evaluate the steady-state solution to the above rate equations by setting the time derivatives to zero. To emphasize certain features, we ignore saturation and

assume a degeneracy of unity for all levels. The net power density is then obtained as:

$$P_{\text{net}} = \alpha I \left(1 - \eta_{\text{q}} \frac{h\nu_{\text{f}}}{h\nu}\right) + \alpha_{\text{b}} I \,, \tag{1.5}$$

where $\eta_{\text{q}} = (1 + W_{\text{nr}}/W_{\text{rad}})^{-1}$ is the (internal) quantum efficiency and $h\nu_{\text{f}}$ denotes the mean fluorescence energy of the four-level system given by:

$$h\nu_{\text{f}} = h\nu + \frac{\delta E_{\text{g}}}{2} + \frac{\delta E_u}{1 + (1 + R/w_2)\mathrm{e}^{\delta E_{\text{u}}/k_{\text{B}}T}} \,. \tag{1.6}$$

The ground-state resonant absorption α is given by:

$$\alpha = \sigma_{12} N_{\text{t}} \left(1 + \mathrm{e}^{\delta E_{\text{g}}/k_{\text{B}}T}\right)^{-1} \,. \tag{1.7}$$

Despite its simplicity, the four-level model reveals essential features of solid-state optical refrigeration. First, (1.7) exhibits diminishing pump absorption due to thermal depletion of the top ground state at low temperatures, $k_{\text{B}}T < \delta E_{\text{g}}$. This implies that the width of the ground-state manifold (δE_{g}) must be narrow to achieve cooling at low temperatures with reasonable efficiency. This issue will be revisited when discussing semiconductors in Section 1.4. Second, (1.6) shows that the mean fluorescence photon energy is redshifted at low temperatures, which further lowers the cooling efficiency. This shift is enhanced if the electron–phonon interaction rate (w_2) is smaller than the upper state recombination rate (R). This means that if $w_2 < R$, the excited state can decay before thermalization with the lattice, which results in no fluorescence upconversion and no cooling [18]. This extreme limit of cold electron recombination is an issue for semiconductors at very low temperatures, where the electrons primarily interact with the lattice via relatively slow acoustic phonons [15].

Dividing (1.5) by the total absorbed power density $P_{\text{abs}} = (\alpha + \alpha_{\text{b}})I$ gives the cooling efficiency $\eta_{\text{c}} = -P_{\text{net}}/P_{\text{abs}}$:

$$\eta_{\text{c}} = \eta_{\text{q}} \eta_{\text{abs}} \frac{h\nu_{\text{f}}}{h\nu} - 1 \,, \tag{1.8}$$

which is similar to (1.1b), not including the luminescence trapping. The most useful feature of the four-level model is its description of the temperature dependence of the cooling in a physically transparent manner. As the temperature is lowered, the redshifting of the mean fluorescence wavelength and the reduction of the resonant absorption reduce the cooling efficiency. At the temperature $T = T_{\text{m}}$, the cooling stops (i.e. $\eta_{\text{c}}\,(T_{\text{m}}) = 0$). This minimum achievable temperature (T_{m}) can be lowered by reducing the background absorption (higher purity), increasing the quantum efficiency, and enhancing the resonant absorption (e.g. choosing a material with a narrow ground-state manifold). The effect of fluorescence trapping and its consequent reabsorption by both resonant and parasitic processes will further diminish the quantum efficiency. We will discuss this in detail when we analyze laser cooling in semiconductors where total internal reflection leads to substantial trapping.

1.3
Cooling Rare-Earth-Doped Solids

The advantages of rare-earth (RE)-doped solids for laser cooling had been foreseen for decades. Kastler (1950) [11] and Yatsiv (1961) [13] suggested that these materials could be used for optical cooling. The key optical transitions in RE-doped ions involve 4f electrons that are shielded by the filled 5s and 6s outer shells, which limit interactions with the surrounding lattice. Nonradiative decays due to multiphonon emission are thus suppressed. Hosts with low phonon energy (e.g. fluoride crystals and glasses) further diminish nonradiative decay and hence boost quantum efficiency. In 1968, Kushida and Geusic [12] attempted to cool a Nd^{3+}:YAG crystal with 1064 nm laser radiation. They reported a reduction in heating but no cooling; it is unclear whether they observed any anti-Stokes cooling effects. Laser cooling of a solid was first experimentally demonstrated in 1995 with the ytterbium-doped fluorozirconate glass ZBLANP:Yb^{3+} [14]. Laser-induced cooling has since been observed in a range of glasses and crystals doped with Yb^{3+} (ZBLANP [19–22], ZBLAN [23, 24], CNBZn [9, 25] BIG [25, 26], $KGd(WO_4)_2$ [9], $KY(WO_4)_2$ [9], YAG [27], Y_2SiO_5 [27], KPb_2Cl_5 [25,28], BaY_2F_8 [29–31], and YLF [32, 33]). See also Chapters 2–5 for further reading on this subject, ranging from synthesis to practical implementations of optical refrigeration in various rare-earth-doped solids.

Figure 1.4 shows the cooling and heating of a sample of Yb^{3+}-doped ZBLANP for a range of pump wavelengths. The data in Figure 1.4 were obtained using a setup similar to that of Figure 1.2, where the pump laser is circulated in a nonresonant cavity by bouncing off dielectric mirrors deposited on the sample [5]. For wave-

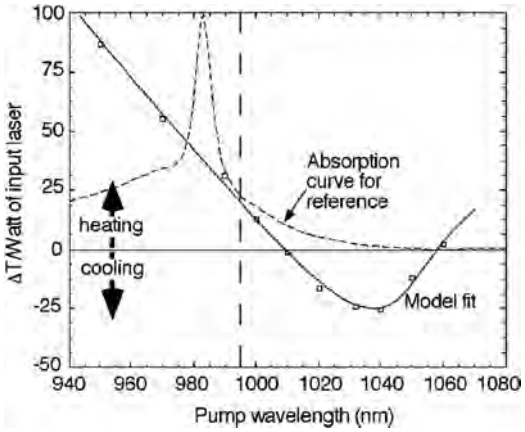

Figure 1.4 The temperature change (normalized to the incident power) in ytterbium-doped ZBLANP glass as a function of pump wavelength. When the pump wavelength is considerably longer than the mean wavelength of the fluorescence λ_F (*vertical dashed line*), the escaping light carries more energy than the absorbed laser light and the glass cools. Heating at wavelengths greater than λ_F is due to the imperfect quantum efficiency of the fluorescence and nonresonant light absorption [5].

lengths that are shorter than the mean fluorescence wavelength λ_F (vertical dashed line), the sample heats up due to the Stokes shift as well as nonradiative processes. At longer wavelengths, anti-Stokes cooling dominates, and cooling as large as 25 K/W of absorbed laser power is measured. At still longer wavelengths, absorption by impurities or imperfections dominates, and the sample heats.

In 2000, laser cooling in Tm^{3+}-doped ZBLANP was reported at $\lambda \sim 1.9$ µm [34]. The significance of this result was twofold. First, it verified the scaling law of (1.1a) and (1.1b) by demonstrating that there was a factor of almost two enhancement in the cooling efficiency compared to Yb-doped systems. The enhancement scales as the ratio of the corresponding cooling transition wavelengths. Second, it was the first demonstration of laser cooling in the presence of excited state absorption. A record cooling power of ~ 73 mW was obtained in this material by employing a multipass geometry [35]. More recently, cooling of Er^{3+}-doped glass (CNBZn) and crystal (KPb_2Cl_5) at $\lambda \sim 0.870$ µm was reported by a Spanish group ([36], see also Chapter 4 for more details). It is interesting to note that the cooling transition used in these experiments is between the ground state and the fourth excited state ($^4I_{9/2}$) of Er^{3+}, not the first excited state as illustrated in Figure 1.1. High-energy transitions have lower cooling efficiencies (1.1) but potentially higher quantum efficiencies due to their low nonradiative decay rates to the ground state. The presence of higher excited states in Er^{3+} may prove advantageous, since the energy upconversion transitions (i.e. at the cooling wavelengths of the main transition) are endothermic, with a high quantum efficiency [36, 37]. This is also the case with the cooling of Tm^{3+} [34].

The initial proof-of-principle experiments in ZBLANP:Yb^{3+} achieved cooling by an amount of 0.3 K below ambient temperature [14]. The LANL group has since cooled ZBLANP:Yb^{3+} to 208 K starting from room temperature [22], as shown in Figure 1.5. Although progress is being made, optical refrigerators need to be more efficient and operate at lower temperatures, below about 170 K, to be competitive with other solid-state coolers such as thermoelectric (Peltier) devices. Several studies have shown that ytterbium- or thulium-doped solids should be capable of providing efficient cooling at temperatures well below 100 K [4, 27, 38].

There are several factors that limit the cooling of rare-earth-doped solids in available materials. The most significant factor is the choice of laser-cooling medium. The ideal cooling efficiency (1.1) shows that there is an advantage of pumping with lower-energy photons. This increased efficiency was part of the motivation for investigating thulium-doped cooling materials, since their ground- and excited-state manifolds are separated by about 0.6 eV, compared to 1.2 eV in ytterbium-doped solids. There are obstacles, however, when moving to longer wavelengths. The first is the limited choice in relation to pump lasers, since there are fewer available near 0.6 eV than near 1.2 eV. While this is not a fundamental consideration, it needs to considered for near-term commercialization. A second and more general reason involves the ratio of radiative to nonradiative relaxation decays. The rate of nonradiative, heat-producing, multiphonon decay decreases exponentially with the separation between the ground- and first excited-state manifolds; this is the well-known energy-gap law. In practical terms, this means that because of the relatively large

energy of the excited level in ytterbium-doped materials, nonradiative decays do not significantly decrease the quantum efficiency. For pure thulium-doped material, nonradiative decay can overwhelm anti-Stokes cooling, depending on the properties of the host material. For materials with low maximum phonon energies, such as ZBLANP and other fluoride hosts, the nonradiative decays are relatively slow. Many thulium-doped oxide crystals and glasses have rapid nonradiative decay rates that prevent laser cooling.

Another consideration in the choice of cooling medium is the width of the ground-state manifold. According to Boltzmann statistics, lower energy levels in the manifold are more populated than higher ones. As the temperature falls and $k_B T$ becomes small compared to the energy width of the ground-state manifold,

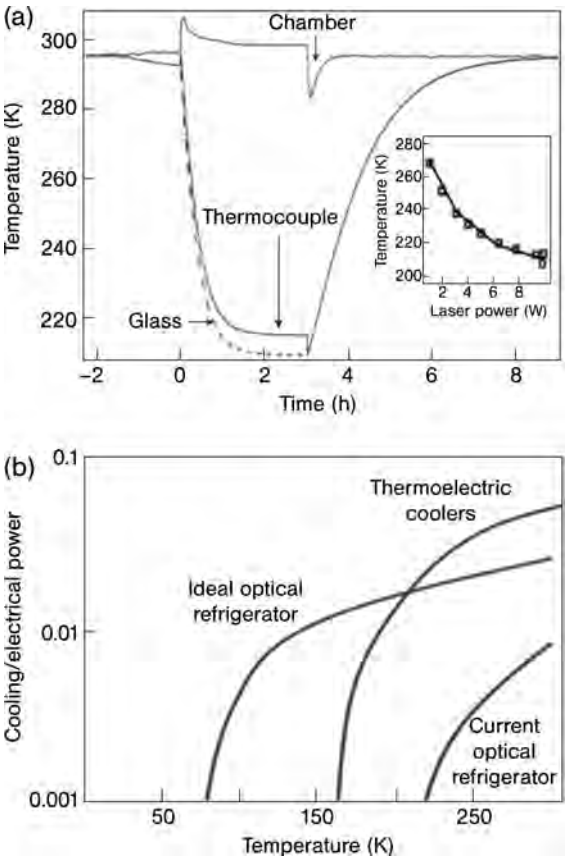

Figure 1.5 Panel (a) shows record cooling to 208 K with ZBLANP:Yb^{3+}. The temperatures are measured with thermocouples on the sample and chamber; the internal temperature of the glass is inferred [22]. Panel (b) compares the cooling efficiencies of available thermoelectric coolers (TECs) with ZBLANP:Yb^{3+}-based optical refrigerators. Devices based on materials with low parasitic heating will outperform TECs below 200. Coolers made from current materials are less efficient than TECs at all temperatures [39]. Figure 1.5a has been reproduced from [22].

the upper levels become depopulated, leading to increased transparency at lower frequencies; this effect is illustrated in the four-level system discussed above. The net effect is that, at low temperatures, the numerator of (1.2) becomes small and cooling efficiency goes to zero; see (1.1b). The width of the ground-state manifold is typically the result of crystal field splitting and depends on both the dopant ion and the host material. By choosing ions and a host that give narrow ground-state manifolds, the material can cool to lower temperatures before the low-frequency transparency condition sets in.

For the material systems studied so far, cooling is not limited by the reasons outlined above. It is most likely hindered by parasitic heating in the bulk of the cooling material or on its surface. As one can see in Figure 1.5b, the cooling efficiencies of currently available ZBLANP:Yb^{3+} are far below that of an ideal material with no parasitic heating. One important source of heating in this material is the quenching of excited ytterbium ions by impurities such as iron and copper. The radiative decay time of an excited Yb^{3+} ion is about 1 ms. During this time, the excitation migrates through the glass by transferring energy to neighboring ions. If the excitation encounters an impurity atom, the energy can be transferred to this atom and rapidly converted into heat. A detailed study by Hehlen *et al.* [39] found that the ideal cooling efficiency can be approached when the concentration of an impurity such as Cu^{2+} is less than 0.01 ppm and that for Fe^{2+} is below 0.1 ppm; see Figure 1.6. See also Chapter 2 by Hehlen.

An additional source of parasitic heating is absorption in the mirrors that trap the pump radiation in the cooling element. In the LANL experiments, the cooling glass has a pair of high-reflectivity mirrors deposited on two surfaces, as depicted in Fig-

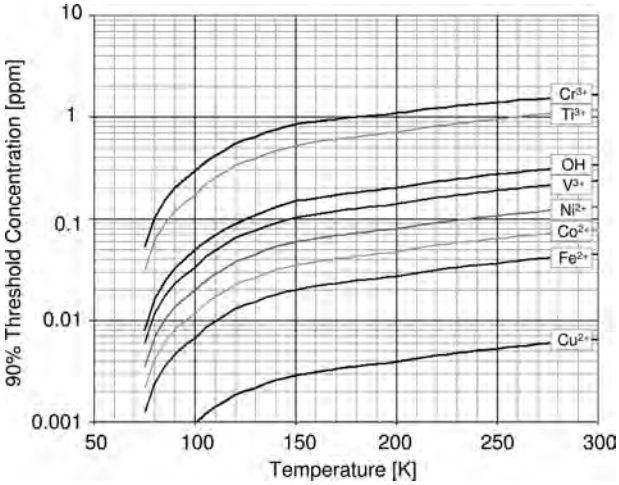

Figure 1.6 Calculated impurity threshold concentrations. If the impurity level of an ion is above the level shown here, the cooling efficiency of the ZBLAN:1%Yb^{3+} will be less than 90% of its ideal value and rapid heat conversion can occur. See the detailed study by Hehlen *et al.* [39].

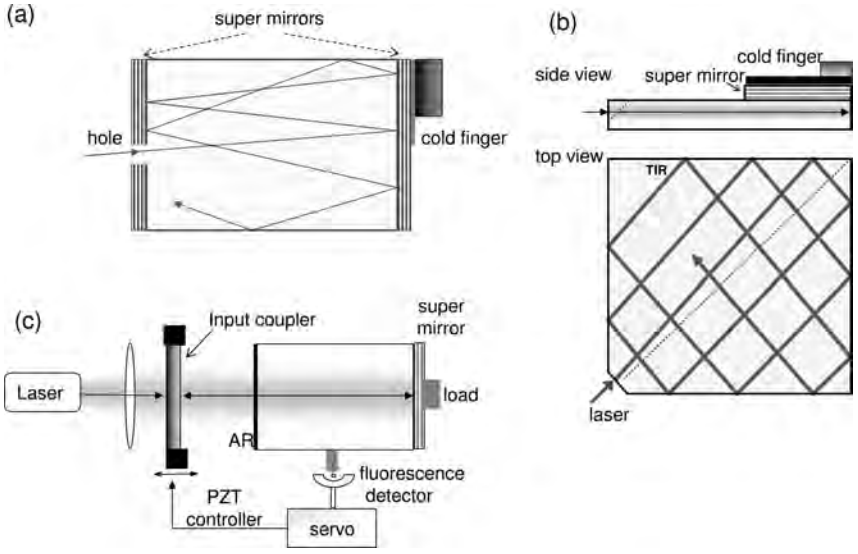

Figure 1.7 Methods to enhance pump absorption. (a) Nonresonant cavity formed by dielectric mirrors deposited on the sample. The pump laser enters through a small hole in one of the mirrors. (b) Nonresonant cavity based on total internal reflection, in which the laser enters through a bevel. (c) Cavity-enhanced absorption, where light couples through a matched dielectric mirror. This required active stabilization.

ures 1.2 and 1.7a. Pump light is reflected multiple times by each mirror, so that that even a relatively low absorption of 0.0001 per surface produces significant heating. The deposition of higher-quality dielectric mirrors, which is currently undertaken by LANL/UNM teams, should obviate this problem. An alternative approach is to avoid dielectric mirrors altogether and exploit total internal refection to circulate the pump beam, as depicted in Figure 1.7b [40]. A proof-of-concept experiment by UNM demonstrated more than ten roundtrips and $\Delta T \approx 8$ K in Tm:ZBLANP [40]. However, the absorbed power was limited by the imperfections in the right-angle corners, which were found to be difficult to control due to the mechanical properties of ZBLANP. In Chapter 5, Mills and Buchwald discuss another variation of this technique recently investigated by Ball Aerospace Inc. Another method of enhancing pump absorption is to use resonant cavity effects. Both intra-laser-cavity [24] and external resonant cavity [41] geometries have been demonstrated. The latter approach, as depicted in Figure 1.7c, has been found to be capable of achieving pump absorption exceeding 90% [41]. Most recently, this method was employed using active stabilization to successfully achieve $\Delta T \approx 70$ K in a Yb:YLF crystal [33]. This is a highly promising result considering that it was obtained with a full blackbody thermal load that is nearly five times higher than that reported in [22]. It has also been proposed that photon localization in nanocrystalline powders can be exploited to enhance laser pump absorption in the cooling of rare-earth-doped systems [42].

1.4
Prospects for Laser Cooling in Semiconductors

Researchers have examined other condensed matter systems beyond RE-doped materials, with an emphasis on semiconductors [17, 43–46]. Semiconductor coolers provide more efficient pump light absorption, the potential for much lower temperatures, and the opportunity for direct integration into electronic and photonic devices. However, these materials provide their own set of engineering challenges, and net cooling is yet to be observed. The essential difference between semiconductors and RE-doped materials is in their cooling cycles. In the latter, the cooling transition occurs in localized donor ions within the host material, while the former involves transitions between extended valence and conduction bands of a direct gap semiconductor (see Figure 1.8a). Indistinguishable charge carriers in Fermi–Dirac distributions may allow semiconductors to get much colder than RE materials. The highest energy levels of the ground state manifold in the RE-doped systems become less populated as the temperature is lowered, due to Boltzmann statistics. The cooling cycle becomes ineffective when the Boltzmann constant times the lattice temperature becomes comparable to the width of the ground state (see previous section describing the four-level model). This sets a limit of $T \sim 100$ K for most existing RE-doped systems. No such limitation exists in pure (undoped) semiconductors – temperatures as low as 10 K may be achievable [15, 17, 47]. See also Chapter 6 by Rupper, Kwong and Binder.

Semiconductors should achieve a higher cooling power density than RE materials. The maximum cooling power density (rate of heat removal) is $\approx N \times k_B T/\tau_r$, where N is the photoexcited electron (hole) density and τ_r is the radiative recombination time. In semiconductors, the optimal density N is limited due to many-body processes and does not exceed that of moderately doped RE systems. We can gain

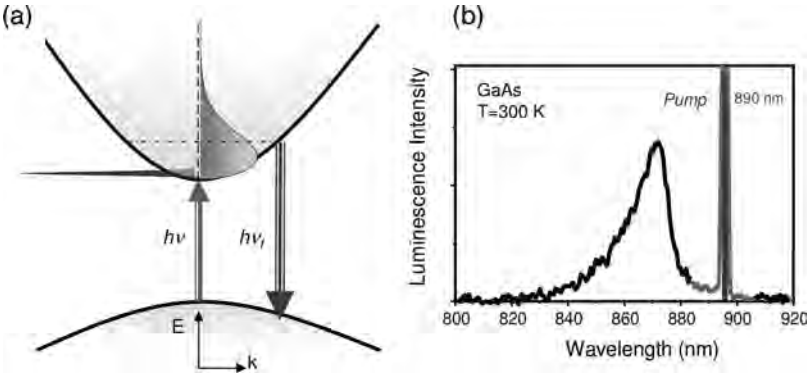

Figure 1.8 (a) Cooling cycle in the laser refrigeration of a semiconductor in which the absorption of laser photons with energy $h\nu$ creates a cold distribution of electron–hole carriers (only the electron distribution is shown for clarity). The carriers then heat up by absorbing phonons, and this is followed by an upconverted luminescence at $h\nu_F$. (b) Typical anti-Stokes luminescence observed in a GaAs/GaInP double heterostructure [6].

5–6 orders of magnitude in cooling power density because the radiative recombination rates in semiconductors are much faster than in RE ions.

Laser cooling of semiconductors has been examined theoretically [15, 44, 45, 47–52], as well as in experimental studies [46, 53–56]. A feasibility study by the authors outlined the conditions needed for net cooling based on fundamental material properties and light management [15]. Researchers at the University of Arizona ([47, 50], Chapter 6) studied luminescence upconversion in the presence of partially ionized excitons, which are understood to attain temperatures approaching 10 K. The role of bandtail states [52] and the possible enhancement of laser cooling by including the effects of photon density of states as well as novel luminescence coupling schemes based on surface plasmon polaritons [57, 58] were recently introduced by Khurgin at Johns Hopkins University. Further details on these issues can be found in Chapter 7 by Khurgin. Here, we expand on the basic model of [15] and present the theoretical foundation of laser cooling in semiconductor structures with an arbitrary external efficiency. This treatment accounts for the luminescence redshift due to reabsorption, the effect of the parasitic absorption of the pump, the luminescence power, and band-blocking effects. We then discuss the latest experimental results from attempts to achieve the first observations of laser cooling in a semiconductor material.

We consider an intrinsic (undoped) semiconductor system uniformly irradiated with laser light at photon energy $h\nu$. Furthermore, we assume that only a fraction η_e of the total luminescence can escape the material while the remaining fraction $(1-\eta_e)$ is trapped and recycled, thus contributing to carrier generation. For now, we will ignore the parasitic absorption of luminescence, but we will consider its implications later. For a given temperature, the rate equation for the electron–hole pair density (N) is given by [15]:

$$\frac{dN}{dt} = \frac{\alpha I}{h\nu} - AN - BN^2 - CN^3 + (1-\eta_e)BN^2 \ . \tag{1.9}$$

Here $\alpha(\nu, N)$ is the interband absorption coefficient, which includes many-body and blocking factors. The recombination process consists of nonradiative (AN), radiative (BN^2), and Auger (CN^3) rates. All of the above coefficients are temperature dependent. The last term represents the increase in N from the reabsorption of the luminescence that does not escape, assuming that the reabsorption occurs within the laser excitation volume. The density dependence of α results from both Coulomb screening and band-blocking (saturation) effects. The latter can be approximated by a blocking factor such that [59, 60]:

$$\alpha(N, h\nu) = \alpha_0(N, h\nu)\{f_v - f_c\} \ , \tag{1.10}$$

where α_0 denotes the unsaturated absorption coefficient. The strongly density-dependent blocking factor in the parentheses [61] contains Fermi–Dirac distribution functions for the valence (f_v) and conduction (f_c) bands.

Under steady-state conditions, (1.9) can be rewritten as

$$0 = \frac{\alpha(\nu, N)}{h\nu} I - AN - \eta_e BN^2 - CN^3 \ . \tag{1.11}$$

This indicates that the fluorescence trapping effectively inhibits the spontaneous emission as it appears through $\eta_e B$ only. This result has also been shown previously by Asbeck [16]. It is important to note that η_e is itself an averaged quantity over the entire luminescence spectrum.

$$\eta_e = \frac{\int S(\nu) R(\nu)\, d\nu}{\int R(\nu)\, d\nu} \,. \tag{1.12}$$

Here $S(\nu)$ is the geometry-dependent escape probability of photons with energy $h\nu$, and $R(\nu)$ is the luminescence spectral density, which is related to the absorption coefficient through reciprocity using a "nonequilibrium" van Roosbroeck–Shockley relation (also known as the Kubo–Martin–Schwinger (KMS) relation) [59, 62]:

$$R(\nu, N) = \frac{8\pi n^2 \nu^2}{c^2} \alpha(\nu, N) \left\{ \frac{f_c(1 - f_v)}{f_v - f_c} \right\}, \tag{1.13}$$

where c is the speed of light and n is the index of refraction. Note that the radiative recombination coefficient B is obtained by $BN^2 = \int R(\nu)\, d\nu$, which results in a negligible dependence of B on N at the carrier densities of interest. The net power density that is deposited in the semiconductor is the difference between the power absorbed from the laser (P_{abs}) and that of the luminescence that escapes (P_{le}):

$$P_{net} = P_{abs} - P_{le} = [\alpha I + \Delta P] - \left[\eta_e B N^2 h\tilde{\nu}_f\right], \tag{1.14}$$

where the absorbed power density includes the resonant absorption (αI) and a term ΔP that accounts for the undesirable effects such as free-carrier absorption and other parasitic absorptive processes. The second term is the escaped luminescence power density at a mean luminescence energy $h\tilde{\nu}_f$, defined as

$$h\tilde{\nu}_f = \frac{\int S(\nu) R(\nu) h\nu\, d\nu}{\int S(\nu) R(\nu)\, d\nu} \,. \tag{1.15}$$

Note that the escaped mean luminescence energy can deviate (i.e. redshift) from its internal value ($S = 1$) depending on the thickness or photon recycling conditions. With the aid of (1.9), we rewrite (1.14) as:

$$P_{net} = \eta_e B N^2 (h\nu - h\tilde{\nu}_f) + ANh\nu + CN^3 h\nu + \Delta P \,. \tag{1.16}$$

Equation 1.16 rigorously describes the laser cooling of a semiconductor in a compact and simple form. It accounts for the practical considerations of luminescence trapping by introducing an inhibited radiative recombination ($\eta_e B$) and a shifted mean photon energy $h\tilde{\nu}_f$ for the escaped luminescence. For high external efficiency systems where $S(\nu) = 1$, (1.16) approaches that described in the literature with $\eta_e = 1$ and $\tilde{\nu}_f = \nu_f$, where ν_f denotes the mean fluorescence energy produced internally in the semiconductor [44–46]. Equation 1.16 indicates that laser cooling occurs when $P_{net} < 0$, requiring a dominant contribution from the radiative recombination with $h\nu < h\tilde{\nu}_f$. The cooling efficiency η_c is defined as the ratio of cooling

power density $P_c(=-P_{net})$ to the absorbed laser power density ($P_{abs} = \alpha I + \Delta P$). With the aid of (1.11), this efficiency can be expressed as

$$\eta_c = -\frac{\eta_e BN^2(h\nu - h\tilde{\nu}_f) + ANh\nu + CN^3 h\nu + \Delta P}{\eta_e BN^2 h\nu + ANh\nu + CN^3 h\nu + \Delta P} . \tag{1.17}$$

Ignoring the ΔP contributions for the moment, η_c can be written more simply as:

$$\eta_c = \eta_{ext}\frac{\tilde{\nu}_f}{\nu} - 1 , \tag{1.18}$$

where η_{ext} describes the *external* quantum efficiency (or EQE):

$$\eta_{ext} = \frac{\eta_e BN^2}{AN + \eta_e BN^2 + CN^3} \approx (\eta_q)^{1/\eta_e} , \tag{1.19}$$

with $\eta_q = BN^2/(AN + BN^2 + CN^3)$ denoting the *internal* quantum efficiency [46, 63], and defined more generally following (1.5). The approximate equality in (1.19) is valid only when η_{ext} is close to unity (> 0.9). One simple consequence of (1.19) is that there is an optimum carrier density $N_{op} = (A/C)^{1/2}$ at which η_{ext} reaches a maximum:

$$\eta_{ext}^{max} = 1 - \frac{2\sqrt{AC}}{\eta_e B} . \tag{1.20}$$

The inclusion of the background parasitic absorption ($\Delta P = \alpha_b I$) results in a more general form for the cooling efficiency:

$$\eta_c = \eta_{abs}\eta_{ext}\frac{\tilde{\nu}_f}{\nu} - 1 , \tag{1.21}$$

where the absorption efficiency η_{abs} is the fraction of all of the absorbed photons from the pump laser that are consumed by the resonant absorption in the cooling region:

$$\eta_{abs} = \frac{\alpha(\nu)}{\alpha(\nu) + \alpha_b} , \tag{1.22}$$

and α_b is assumed to be constant in the vicinity of the band-edge region.

If the pump laser suffers from parasitic absorption, so will the luminescence, since their frequencies are very close. We now examine the parasitic absorption problem and its effect on the cooling efficiency by revisiting (1.9). A small fraction ε_f of the trapped luminescence is absorbed parasitically and the remaining part $(1 - \varepsilon_f)$ is recycled through interband absorption, thus contributing to carrier generation. Equation 1.9 is rewritten as:

$$\frac{dN}{dt} = \frac{\alpha I}{h\nu} - AN - BN^2 - CN^3 + (1 - \eta_e)(1 - \varepsilon_f)BN^2 . \tag{1.23}$$

Note that $1 - \varepsilon_f = \bar{\alpha}_f/(\bar{\alpha}_f + \alpha_b) \approx 1 - \alpha_b/\bar{\alpha}_f$ where $\bar{\alpha}_f(\approx \alpha(\nu_f))$ is the interband absorption of the luminescence averaged over its spectrum. Following the same analysis leading to (1.21), we obtain the modified cooling efficiency:

$$\eta_c = \bar{\eta}_{ext}\eta_{abs}\frac{\bar{\nu}_f}{\nu} - 1 , \tag{1.24}$$

with a modified EQE ($\tilde{\eta}_{\text{ext}}$) that is reduced from its ideal value in the high-purity ($\alpha_{\text{b}} \approx 0$) approximation to:

$$\tilde{\eta}_{\text{ext}} = \eta_{\text{ext}} \frac{1}{1 + \eta_{\text{ext}} \varepsilon_{\text{f}} (1 - \eta_{\text{e}})/\eta_{\text{e}}} \approx \eta_{\text{ext}} - \eta_{\text{ext}}^2 \varepsilon_{\text{f}} (1 - \eta_{\text{e}})/\eta_{\text{e}} \,. \tag{1.25}$$

This expression is useful for setting an upper bound on the existing intrinsic background absorption of GaAs/InGaP heterostructures. This will be discussed in detail below. Parasitic luminescence absorption is not important in the analysis of photocarrier density and incident laser irradiance, so it is ignored for the moment.

The roots of (1.16) define the carrier density range within which net cooling can be observed provided that $\eta_{\text{e}} B(h\tilde{\nu}_{\text{f}} - h\nu) \geq 2h\nu\sqrt{AC}$. The equality defines the break-even condition: heating and cooling are in exact balance. At high quantum efficiency, radiative recombination dominates (i.e. $\eta_{\text{e}} B/C \gg N \gg A/\eta_{\text{e}} B$), allowing one to obtain the corresponding laser irradiance from (1.11) with the assumption of no band blocking. We can account for parasitic absorption of the pump by taking $\Delta P = \alpha_{\text{b}} I + \sigma_{\text{fca}} N I$, where α_{b} denotes an *effective* background parasitic absorption and σ_{fca} is the free carrier absorption cross-section. In this case, net cooling can occur within an irradiance range of $I_1 < I < I_2$, where $I_{1,2} = (h\nu\eta_{\text{e}} B/\alpha(\nu))n_{1,2}^2$ and

$$N_{1,2} = \left(\frac{h\tilde{\nu}_{\text{f}} - h\nu}{h\nu} - \frac{\alpha_{\text{b}}}{\alpha(\nu)} \right) \frac{\eta_{\text{e}} B}{2C'} \left(1 \mp \sqrt{1 - \frac{A}{A_0}} \right) . \tag{1.26}$$

Here $C' = C + \sigma_{\text{fca}} \eta_{\text{e}} B/\alpha(\nu)$, and

$$A_0 = \left(\frac{h\tilde{\nu}_{\text{f}} - h\nu}{h\nu} - \frac{\alpha_{\text{b}}}{\alpha(\nu)} \right)^2 \frac{(\eta_{\text{e}} B)^2}{4C'} \,, \tag{1.27}$$

is the break-even (maximum allowable) nonradiative decay rate for a given excitation energy $h\nu$. Free carrier absorption appears as an enhancement of the Auger process. The parameters B and C are fundamental properties of a semiconductor and have been calculated and measured extensively for various bulk and quantum-confined structures [59, 60, 63, 64]. The reported values for these coefficients, however, vary considerably. In bulk GaAs, for example, the published values are $2 \times 10^{-16} < B < 7 \times 10^{-16}\,\text{m}^3/\text{s}$ and $1 \times 10^{-42} < C < 7 \times 10^{-42}\,\text{m}^6/\text{s}$ [64]. These variations are primarily due to experimental uncertainties. We assume average values of $B = 4 \times 10^{-16}\,\text{m}^3/\text{s}$ and $C = 4 \times 10^{-42}\,\text{m}^6/\text{s}$ while ignoring the effects of background and free-carrier absorption. These assumptions allow us to gain insight into the feasibility and requirements for achieving net laser cooling. It should be noted that the theoretical values obtained for these parameters with different models vary within almost the same range as the experimental results. For the simple two-band model used here, $B \approx 5 \times 10^{-16}\,\text{m}^3/\text{s}$ [65].

Using (1.27), we plot in Figure 1.9 the break-even nonradiative lifetime $\tau_{\text{nr}}^0 = A_0^{-1}$ as a function of η_{e} assuming $h\nu_{\text{f}} - h\nu = k_{\text{B}} T$, with $h\nu_{\text{f}}$ corresponding to $\lambda_{\text{f}} \approx 860$ nm

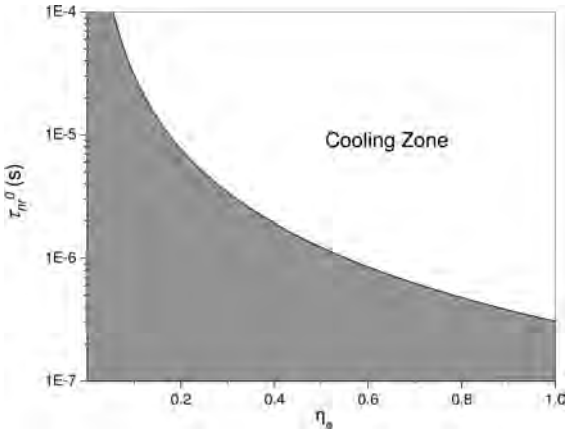

Figure 1.9 The break-even nonradiative lifetime as a function of the luminescence extraction efficiency in bulk GaAs, calculated using typical values of radiative and Auger recombination at room temperature.

at room temperature. The orange area under the curve is the unwanted (heating) zone. Equation 1.27 also suggests that increasing the quantum efficiency η_q by decreasing the incident photon energy (e.g. at $h\nu_f$–$h\nu > k_B T$) relaxes this requirement. Interband absorption drops rapidly as the excitation moves further into the Urbach tail and the background and free carrier absorption can no longer be ignored. Recently, it was found that the free-carrier absorption (FCA) at band-edge wavelengths is much smaller than previously expected [66,67]. For GaAs, $\sigma_{fca} \approx 10^{-24}$ m^2 [66,67], which requires that $\alpha(\nu) \geq 10^3$ m^{-1} to ensure that free carrier losses are negligible (i.e. $C' \approx C$). This requirement is satisfied even at $\lambda = 890$ nm (corresponding to $h\nu_f - h\nu \approx 2k_B T$), where $\alpha(\nu) \approx 10^4$ m^{-1}. We conclude that FCA does not place a limitation on laser cooling.

We can categorize the possible sources and locations of the parasitic background absorption α_b into three regions: (a) active or core material, (b) cladding layers of the heterostructure, and (c) the substrate. It is also implicit that α_b in (1.27) is scaled such that, for cases (b) and (c), the actual background absorption coefficient $\alpha_b' = \alpha_b \times (d/L)$, where d and L are the thicknesses of the loss and active media (if different), respectively.

While situations (b) and (c) can be controlled experimentally by varying the barrier thickness or using high-purity substrate respectively, the parasitic absorption from the cooling layer itself presents the most difficult engineering obstacle. This limitation is revisited in the next section, where experiments on laser cooling with GaAs are analyzed.

It is also instructive to show an alternative and compact way of expressing the cooling condition. With laser excitation at $h\nu < h\bar{\nu}_f$, the cooling condition defined by EQE reduces to:

$$\eta_{ext} > \frac{\nu}{\bar{\nu}_f} + \frac{\alpha_b}{\alpha(\nu)} . \tag{1.28}$$

Including the parasitic absorption of luminescence allows us to replace η_{ext} with $\tilde{\eta}_{ext}$, and (1.28) then gives a more general condition,

$$\tilde{\eta}_{ext} = \eta_{ext} - \frac{\alpha_b(1-\eta_e)}{\bar{\alpha}_f \eta_e} > \frac{\nu}{\nu_f} + \frac{\alpha_b}{\alpha(\nu)} . \tag{1.29}$$

The above inequality emphasizes the critical role of α_b in achieving net laser cooling. The quantity $\tilde{\eta}_{ext}$ can be measured accurately, so (1.28) defines the minimum value of EQE for a given background absorption, provided $\alpha(\nu)$ is known. The absorption $\alpha(\nu)$ drops sharply for energies considerably below the bandgap, which means that this inequality may never be satisfied for any wavelength if α_b is too large. To quantify this argument, we need to know the band-tail absorption accurately. The nature of the band-tail states and their dependence on the impurity type and concentration make the reported experimental values very sample specific. Most theoretical calculations are accurate only for above and near the bandgap wavelengths. It is best to approach the problem experimentally with absorption and luminescence data that allow accurate estimates of the required EQE using (1.9). Starting with the measured low-density photoluminescence (PL) spectrum on a high-quality sample, we obtain absorption spectra $\alpha(\nu)$ using the KMS relations of (1.13). The low-density approximation reduces the occupation factor to a simple Boltzmann factor, $\exp(-h\nu/k_B T)$, where we ignore possible band-filling (saturation) effects in the band tail. Using (1.9), the minimum η_{ext} required can be estimated as a function of $h\nu$ for various values of α_b, as depicted in Figure 1.10. Here we assume an extraction efficiency $\eta_e = 0.1$, which is typical of GaAs on a ZnS dome structure [15, 68].

Figure 1.10 indicates that the required EQE for cooling becomes more demanding as the temperature is lowered, which is essentially a consequence of the diminishing phonon population at low temperatures. This result mirrors the situation in

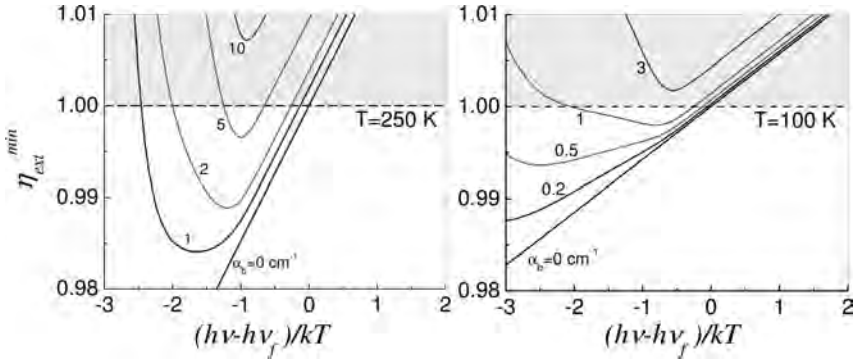

Figure 1.10 The minimum EQE required to achieve laser cooling versus the normalized excitation photon energy for GaAs at $T = 250$ and 100 K, obtained from the inequality of (1.29). The absorption data $\alpha(\nu)$ were obtained by using the KMS relations on the PL spectra on a high-quality GaAs/InGaP double heterostructure. Note that for a certain background absorption α_b, the requirement $\eta_{ext} > 1$ is unattainable (nonphysical) for any wavelength. This restriction becomes more prevalent at lower temperature.

the rare-earth-doped materials. Semiconductors, however, have the fortunate property that their EQE increases with decreasing temperature. The loss terms (A and C coefficients) decrease while the radiative rate (B coefficient) increases inversely with lattice temperature. Using the accepted scaling for $C(T) \propto \exp(-\beta(300/T-1))$ with $\beta \approx 2.4$ for GaAs [55,69], taking $B \propto T^{-3/2}$ [59,70], keeping $h\tilde{\nu}_f/h\nu - 1 \approx k_B T/E_g$, and ignoring parasitic losses and the small temperature dependence of the bandgap energy, we obtain for the break-even nonradiative decay rate

$$\frac{A_0(T)}{A_0(300)} \approx \left(\frac{300}{T}\right) \exp\left(\frac{\beta(300-T)}{T}\right). \tag{1.30}$$

At $T = 150$ K, for example, the break-even lifetime is ~ 40 times lower than it is at room temperature ($T = 300$ K). This is visualized by plotting η_{ext} versus T, as shown in Figure 1.11 for two values of η_e. This range of values of η_e corresponds to a GaAs structure bonded to a high refractive index dome of ZnS or ZnSe [15,68]. The solid red line indicates the break-even condition described by (1.2). This condition, together with the fact that A (typically dominated by surface recombination) increases with temperature [70–72], makes the low-temperature observation of laser cooling more favorable even though the overall efficiency ($\approx k_B T/E_g$) decreases. The reduction in cooling efficiency is effectively due to the reduction of the electron–phonon absorption probability at lower temperatures. In particular, the population of LO phonons yields a corresponding reduction of the exciton linewidth Γ [59]:

$$\Gamma(T) = \Gamma_0 + \sigma T + \gamma N_{LO}(T), \tag{1.31}$$

where Γ_0 is due to impurities and inhomogeneous broadening, σ accounts for the contribution of acoustic phonons, γ is the coefficient of LO-phonon scattering, and $N_{LO}(T)$ denotes the corresponding Bose–Einstein phonon distribution. For the exciton densities involved, we can ignore possible broadening due to exciton–exciton

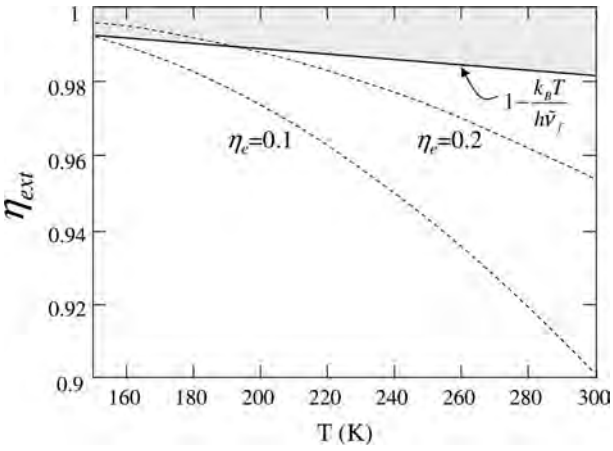

Figure 1.11 The required external quantum efficiency (EQE) as a function of temperature for GaAs under typical parameters.

scattering [73]. As the lattice temperature approaches 10 K, the acoustic phonon contribution begins to dominate. At such low temperatures, however, the exciton–phonon scattering rate ($\approx \Gamma$) becomes comparable to the radiative recombination rate (BN^2) and consequently cold exciton recombination occurs before complete thermalization with the lattice. Similar processes that are related to premature hot exciton recombination have also hindered experimental observations of Bose–Einstein condensation in semiconductors. This problem is significantly alleviated by employing quantum-confined systems where σ is enhanced by nearly three orders of magnitude. This relaxes wave-vector conservation along the confinement directions [74]. Enhanced cooling in quantum-confined systems may allow operation at temperatures < 10 K.

Another issue of concern is absorption saturation (band blocking) and many-body interactions. Band blocking may be a limiting factor for long-wavelength excitation where the low density of states gives rise to a stronger bleaching of the interband absorption. It is therefore necessary to have a good understanding of the absorption and emission spectra and their dynamic nonlinearities.

Theoretical models exist that deal with absorption spectra of semiconductor structures under various carrier densities and lattice temperatures. With different levels of complexity, there are theoretical calculations for 2D and 3D systems that deal with such many-body processes under dense e–h excitation [75–78]. Recently, a rigorous microscopic theory for absorption and luminescence in bulk semiconductors that includes the effects of electron–hole (e–h) plasma density as well as excitonic correlations has been introduced under the quasi-thermal equilibrium approximation [47, 79]. The reader is referred to the above sources for the details. Here, we use a simple model to estimate the effect of band blocking on achieving the carrier densities of (1.26) for GaAs. Using the electron–hole density of

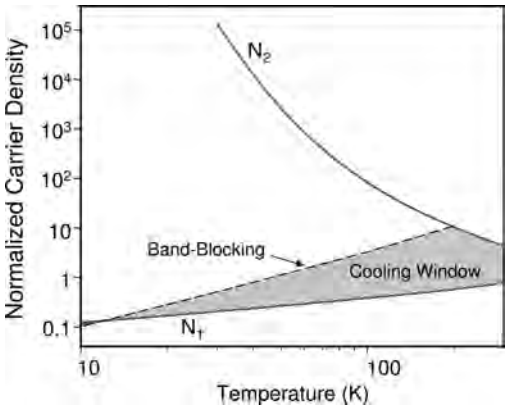

Figure 1.12 The upper carrier density N_2, given by (1.26), is seen to be unattainable in GaAs due to band blocking as the temperature is lowered below 200 K. The *middle (dashed) line* represents the calculated density at which the band-tail absorption at $h\nu = h\nu_f - k_B T$ completely saturates (i.e. $\alpha(N) = 0$, (1.10)). This is a worst case scenario for which the nonradiative recombination rate is assumed to be constant with temperature.

states corresponding to a simple two-parabolic-band model, we calculate the carrier density at which the occupation factor $\{f_v - f_c\}$ vanishes at $h\nu = h\nu_f - k_B T$. The result is depicted in Figure 1.12, where this blocking density is contrasted with N_1 and N_2 of (1.26), evaluated using a constant A coefficient and the temperature-dependent B and C coefficients used earlier. It is seen that band-blocking tends to reduce the cooling density window at $T < 200$ K and that cooling densities become unattainable at $T \approx 10$ K. The simple model overestimates band-blocking effects but qualitatively agrees with the more rigorous microscopic theory [47, 79]. Most recently, Khurgin presented a thorough analysis of the phonon-assisted band-tail states and the role of band blocking using a density matrix approach [52]. In that context, he pointed out the significance of the excitation wavelength in the presence of band blocking (saturation), which tends to diminish the cooling efficiency predominantly for $T \leq 100$ K [52].

Further details on the fundamental theory of laser cooling in semiconductors can be found in Chapters 6 and 7.

1.5 Experimental Work on Optical Refrigeration in Semiconductors

The first thorough experimental effort was reported by the University of Colorado [46]. No net cooling was achieved, despite the realization of an impressive external quantum efficiency of 96% in GaAs. These experiments used a high-quality GaAs heterostructure that was optically contacted with a ZnSe dome structure for enhanced luminescence extraction. A report of local cooling in AlGaAs quantum wells by a European consortium [53] was later attributed to misinterpretation of spectra caused by Coulomb screening of the excitons [80]. Figure 1.8b displays anti-Stokes luminescence in a GaAs heterostructure, where excitation at $\lambda = 890$ nm produces broadband luminescence with a mean wavelength of $\lambda_f \approx 860$ nm. Each luminescent photon carries away about 40 meV more energy than an absorbed photon, so one might expect cooling. Why then have we not been able to observe laser cooling in this material or any semiconductor? To answer this question we have to revisit the cooling condition of (1.2), where strict requirements on EQE and background absorption are yet to be met. As discussed earlier, GaAs currently appears to be most promising due to the mature growth of this technology and its record quantum efficiency. There are, however, challenges that must be overcome to achieve the break-even cooling condition: (a) reduce the surface recombination rate A, (b) reduce the parasitic background absorption α_b, and (c) enhance the luminescence extraction efficiency η_e. Issues (a) and (b) involve material preparation and both concern high-purity growth using advanced epitaxial methods. Condition (c), on the other hand, is a light management and device engineering challenge that deals with luminescence extraction from semiconductors with a high index of refraction. Total internal reflection causes most of the spontaneous emission to get trapped and reabsorbed. A similar problem limits the efficiency of light-emitting diodes (LEDs).

Various methods have been devised to remedy this problem for LEDs, but not all are applicable to laser cooling. For example, photon recycling in thin textured or in photonic bandgap structures can substantially enhance the luminescence extraction but at the price of redshifting the luminescence, as described by (1.15) [15]. Index-matched dome lenses have been exploited for LEDs and can be used for laser cooling as well [46], provided that the dome material does not introduce unacceptable levels of parasitic absorption. This requirement narrows the dome materials for GaAs to nearly index-matched ZnSe and ZnS due to the fact that they are currently available at a high purity grade [81]. GaP substrates or domes can provide a higher η_e due to better index matching to GaAs, but currently available materials produce unacceptable levels of parasitic absorption [81]. Another method of improving η_e makes use of nanosized vacuum gaps (nanogaps), and this will be briefly discussed later [6].

Highly controlled epitaxial growth techniques such as metal organic chemical vapor deposition (MOCVD) can produce very low surface recombination rates ($A < 10^4\ s^{-1}$). This involves a double heterostructure of GaAs/GaInP, as shown in Figure 1.13, where the lattice-matched cladding layers provide surface passivation as well as carrier confinement. To deal with extraction efficiency, geometric coupling schemes such as nearly index-matched dome lenses (also shown in Figure 1.13) have been employed to enhance η_e to 15–20%. The double heterostructures are lithographically patterned into ≈ 1 mm diameter disks that are lifted from their parent GaAs substrates and then bonded via van der Waals forces to a ZnS dome. The EQE of each sample is measured using the technique of fractional heating [46, 68] at various temperatures and laser pump powers.

The experimental setup is shown in Figure 1.14. The pump laser is a cw Ti:sapphire laser producing up to 4.5 W that is tunable in the wavelength range 750 – 900 nm. This laser is pumped by an 18 W laser at 532 nm (Verdi, Coherent Inc.). In the fractional heating experiment, the laser is tuned to around the mean luminescence wavelength while the temperature ΔT of the sample is measured.

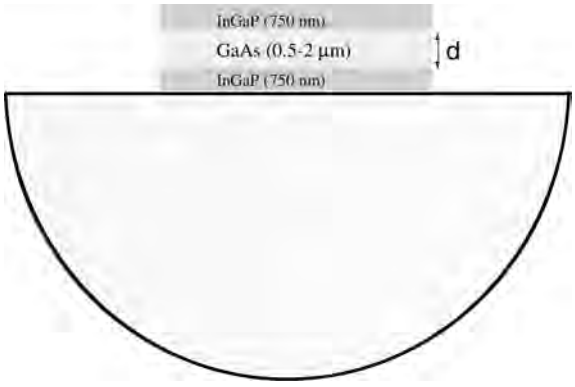

Figure 1.13 The GaAs/GaInP double heterostructure is bonded to a nearly index-matched dome (ZnS or ZnSe) to enhance its luminescence extraction.

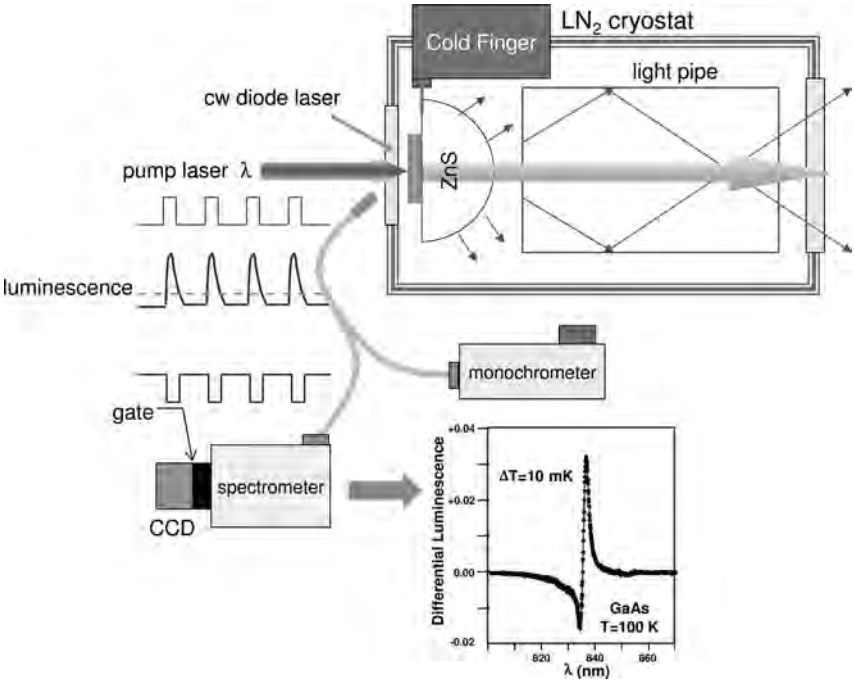

Figure 1.14 Experimental setup for measuring the external quantum efficiency (EQE or η_{ext}) at various lattice temperatures in GaAs/GaInP double heterostructures. A tunable cw laser (Ti:sapphire, 4.5 W) excites a constant density of electron–hole pairs as the pump is tuned near the band edge. This is done by keeping the luminescence intensity (within a certain spectral band) constant using the monochrometer. After recombination, the temperature change of the sample is measured using differential luminescence thermometry (DLT), where the spectral shift of the low-density luminescence spectrum induced by a weak cw laser diode is monitored using the gated spectrometer. The *inset figure* shows a typical DLT signal for $\Delta T = 10$ mK in GaAs at $T = 100$ K.

According to the analysis described earlier, the temperature change in the sample is proportional to the net power deposited, which can be written as:

$$\Delta T(\lambda) = \kappa^{-1} P_{abs}(\lambda) \left(1 - \tilde{\eta}_{ext} \eta_{abs} \frac{\lambda}{\lambda_f}\right), \tag{1.32}$$

where κ is the total thermal conductance (W/K) of the system positioned in an optical cryostat. During the experiment, the absorbed power is kept constant: the pump laser is tuned and its power adjusted to keep the luminescence (or a fixed spectral portion of it) constant. This is shown in Figure 1.14, where a monochrometer is used to monitor the spectral portion of luminescence that does not overlap with the pump wavelength. The temperature change is monitored using a noncontact method called differential luminescence thermometry (DLT) that was developed for this purpose [68]. DLT exploits the temperature dependence of the luminescence resulting from the bandgap shift and broadening. High-temperature sensitivity is obtained by monitoring the differential spectrum before and after pump

irradiation. To avoid complications caused by high carrier density [80], low-density luminescence spectra induced by a weak diode laser generate the DLT signals. This is achieved by modulating the pump laser with a mechanical chopper while synchronously gating a CCD camera on the spectrometer. This ensures that the DLT spectra are recorded when the pump laser is blocked and after the high-density luminescence has decayed. DLT signals are obtained by normalizing the signal and reference spectra before subtraction. The resulting differential signal is a peak–valley or valley–peak feature depending on the sign of ΔT, which is calibrated in situ before an experiment. This method has exhibited a temperature resolution of better than 1 mK [68].

Returning to (1.32), it is evident that if $P_{abs}(\lambda)$ is kept constant, the measured ΔT versus λ follows the wavelength dependence of the cooling (or heating) efficiency represented by the term in the parentheses. At short wavelengths ($\lambda < \lambda_f$) where $\alpha(\lambda)$ is large, η_{abs} can be taken to be unity for moderate to high purity samples, and the fractional heating data follows $\Delta T(\lambda) \propto (1 - \bar{\eta}_{ext}\lambda/\lambda_f)$, which is a straight line. Currently available samples do not possess sufficient purity to make this term negative, i.e. net cooling. When the pump wavelength λ is tuned close to λ_f, α_{abs} tends to degrade, thus preventing net cooling. Extrapolation of the short wavelength data can be used to obtain a "zero-crossing wavelength" λ_c, from which $\bar{\eta}_{ext} = \lambda_f/\lambda_c$ can be deduced. Recall that $\eta_{ext} > \bar{\eta}_{ext}$, and thus we obtain a lower limit on EQE. When parasitic absorption of luminescence can be ignored, $\eta_{ext} \approx \bar{\eta}_{ext}$. In the following analysis of the experimental data, we refer to this lower limit measured by fractional heating technique as the EQE. Figure 1.15a shows the measured EQE for various GaAs layer thicknesses at room temperature. The optimum GaAs thickness is found to be about 1 μm, determined by balancing excessive luminescence reabsorption for thicker layers with dominant surface recombination for thinner layers [55, 82]. The measured temperature dependence of EQE is depicted in Figure 1.15b, which is in qualitative agreement with the earlier analysis. Enhancement is observed as the temperature is lowered, reaching a record 99% at 100 K.

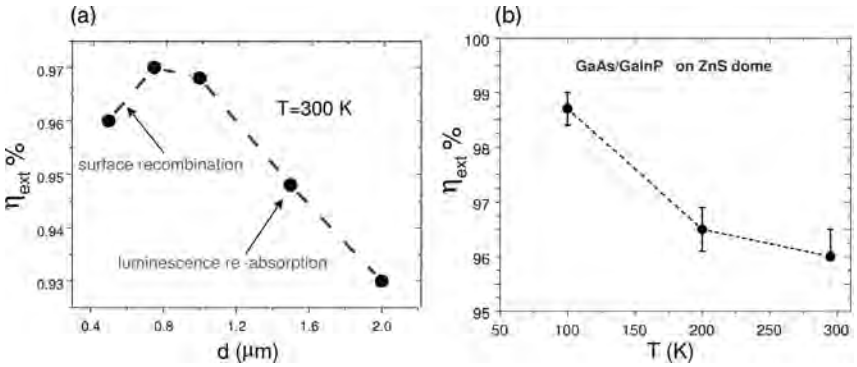

Figure 1.15 External quantum efficiency (EQE) measured with (a) a bonded sample with various GaAs thicknesses, the GaInP layer thickness fixed at 0.5 μm, and $T = 300$ K, and (b) measured EQE vs. lattice temperature for a GaAs thickness of 1 μm.

The fractional heating data leading to 99% EQE is shown in Figure 1.16. We note the increase in temperature at longer wavelengths due to parasitic absorption. With the absorption of GaAs known, the data is fitted with a constant background of $\alpha_b \approx 10\,\mathrm{cm}^{-1}$ assuming that it occurs entirely in the 1 µm thick GaAs layer. The experiment measures $\bar{\eta}_{ext}$, which means that the unmodified EQE (η_{ext}) can be even larger. The average absorption coefficient ($\bar{\alpha}_f \approx 4000\,\mathrm{cm}^{-1}$) allows us to estimate an upper limit for α_b inside the double heterostructure. Even if $\eta_{ext} = 1$, attaining $\bar{\eta}_{ext} = 99\%$ requires that

$$\alpha_b < \frac{(1-\bar{\eta}_{ext})}{(1-\eta_e)/\eta_e}\bar{\alpha}_f \approx 4\,\mathrm{cm}^{-1}\ ,$$

assuming that $\eta_e \approx 0.1$. The value of $\alpha_b = 10\,\mathrm{cm}^{-1}$ that was used to fit the data in Figure 1.16 may include contributions from sources outside the double heterostructure, such as dome or cold-finger contacts.

Experiments show that the external quantum efficiency is sufficient to achieve net laser cooling, but the purity of the samples is not yet high enough. Efforts are underway to address this material problem. Researchers at the National Renewable Energy Laboratory are using highly controlled MOCVD growth, and scientists at the University of New Mexico are exploring aluminum-free GaAs heterostructure growth using phosphorus molecular beam epitaxy (MBE).

Methods of enhancing η_{ext} by improving the luminescence extraction efficiency are also being explored. A novel method based on the frustrated total internal reflection across a vacuum "nano-gap" is being developed at the University of New Mexico [17, 83, 84]. In this scheme, the luminescence photons tunnel through the

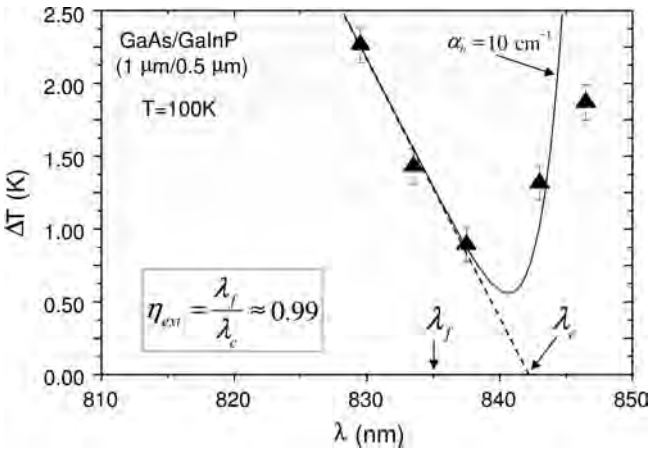

Figure 1.16 Fractional heating of a 1 µm thick GaAs sample as a function of excitation wavelength for a fixed (optimum) electron–hole density at a starting temperature of 100 K. The extrapolation of short-wavelength data determines the zero-crossing wavelength, from which a record EQE of ~ 99% is measured. Excitation at longer wavelengths causes heating due to background parasitic absorption [6, 68].

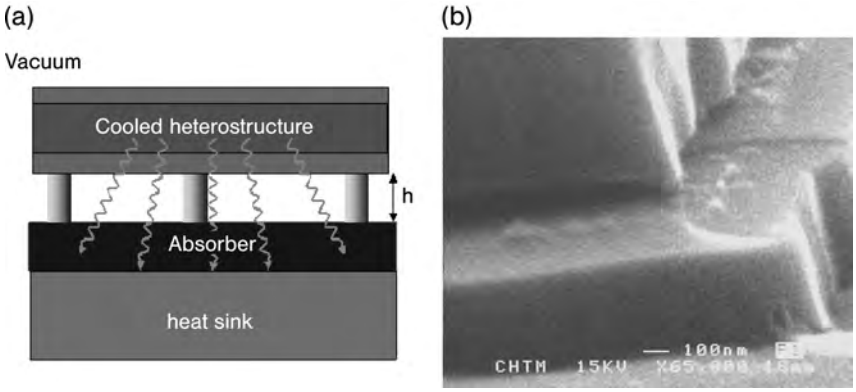

Figure 1.17 (a) A vacuum "nanogap" structure where the heterostructure is situated (e.g. supported by posts) at a subwavelength distance from an absorber. Luminescence photons will escape into the absorber via frustrated total internal reflection (photon tunneling), while the gap provides a thermal barrier. (b) The SEM micrographs of a preliminary nanogap structure (with 50 nm spacing) fabricated using a multistep photolithographic technique [83].

gap into the absorber region. The vacuum nanogap maintains a thermal barrier between the heterostructure and the absorber/heat sink. The cooling heterostructure and the luminescence absorber are thus optically contacted but thermally insulated. Calculations show that a gap spacing of < 25 nm has a higher extraction efficiency than the dome structure (GaAs on ZnS or ZnSe), and the preliminary fabrication of such structures has shown promising results. Using a multistep photolithographic process, a Si-based nanogap with 50 nm spacing supported by posts has been monolithically fabricated, as depicted in Figure 1.17 [83]. Recently, we fabricated GaAs nanogap structures that will be integrated with a high-quality GaAs heterostructure to investigate their performance in cooling experiments.

1.6 Future Outlook

Optical refrigeration has advanced from basic principles to a promising technology. The cooling of rare-earth-based materials is approaching cryogenic operation. In semiconductors, much progress has been made in achieving high external quantum efficiency. With advanced heterostructure growth and novel device fabrication currently underway, cooling will soon be attainable. In the coming years, optical refrigeration will be useful in applications such as satellite instrumentation and small sensors, where compactness, ruggedness and a lack of vibrations are important. Optical refrigeration is well suited to spaceborne applications since it does not involve any moving parts and can be designed for long operational lifetimes. Additionally, the cooling element is not electrically powered, so it will not interfere with the electronics being cooled. One can envision optical refrigerators being

directly integrated with infrared sensors for thermal imaging of the Earth and of astrophysical objects. In terrestrial applications, their small size and high reliability make optical refrigerators attractive for use with high-temperature superconductor sensors and electronics. Optical refrigeration could enable compact SQUID magnetometers for geophysical and biomedical sensing, and may be a critical component in the production of commercial electronics incorporating fast and efficient superconducting components.

Appendix I: Photon Waste Recycling and the Carnot Limit

Many applications will be possible if the basic efficiency of optical refrigerators ~ $k_B T/h\nu$ can be improved. This efficiency limit assumes that all fluorescence photons are absorbed by a heat sink and thus wasted. This is depicted diagrammatically in Figure 1.18a. One expects that overall efficiency will improve if fluorescence photons are recycled with photovoltaic (PV) elements in order to convert them into electricity [85]. This recovered energy can be used to drive laser diodes (LD) at the pump photon energy $h\nu$. This process is shown in Figure 1.18b.

Deriving the new cooling efficiency is then a straightforward process. For the same cooling power (P_c) as in the open loop system, the required laser power in the photon-waste recycled system is lowered by the amount generated by recycling, $\eta_{PV}\eta_L P_f$, where P_f is the luminescence power and η_{PV} and η_L are the power efficiencies of the photovoltaic and the laser diode, respectively. The enhanced cooling efficiency $\tilde{\eta}_c$ is then obtained as

$$\tilde{\eta}_c = \frac{\eta_c}{1 - \eta_{PV}\eta_L(1 - \eta_c)}\,, \tag{1.33}$$

where the "old" or open loop cooling efficiency $\eta_c = 1 - P_f/P_L$, as before. It is useful to investigate what limits this new efficiency. Assuming that η_c is given by its quantum limit of $h\nu_f/h\nu - 1$, we take $h\nu = h\nu_f - mk_B T_c$, where m is on the order of unity and T_c is the temperature of the solid-state coolant. This leads to

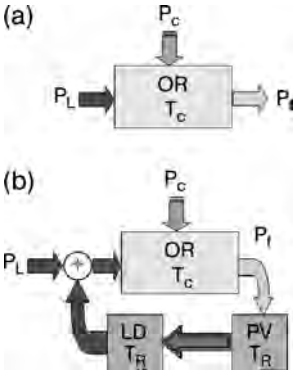

Figure 1.18 Diagrams of (a) an open loop optical refrigerator (OR) and (b) a closed loop system in which the luminescence (photon waste) recycling is performed using photovoltaic (PV) elements followed by a laser diode (LD), both at a temperature T_R.

$\eta_c = mk_B T_c/h\nu_f \approx mk_B T_c/E_g$, where E_g is the energy gap of the transition. The obvious choice for the photovoltaic and laser diode system would be a semiconductor with an energy gap that is very close to E_g. Assuming that both are at a reservoir temperature T_R, it is not unreasonable to take their conversion efficiencies to be $\eta_{PV} = 1 - pk_B T_R/E_g$ and $\eta_L = 1 - qk_B T_R/E_g$, respectively. Current devices reach efficiencies that correspond to $p \approx q \approx 30$–50, so one expects they will be limited by $p \approx q \approx 1$. For such a limit, (1.33) can be written as:

$$\bar{\eta}_c = \frac{T_C}{T_C + \left(\frac{p+q}{m}\right) T_R}. \tag{1.34}$$

We note that thermodynamic analysis requires that $p + q \geq m \approx 1$. With $p + q = m \approx 1$, one obtains the Carnot limit of $T_C/(T_C + T_R)$. Expected technological advances in photovoltaic and laser diode devices will enable efficiencies approaching that corresponding to $p \approx q \approx 1$, and so the ultimate efficiency of the optical refrigerator will be given by its Carnot limit. Further discussions on the thermodynamics of solid-state laser cooling can be found in Chapter 8 by Mungan.

References

1 Chu, S., Cohen-Tannoudji, C. and Philips, W.D. (**1997**) Nobel Prize in Physics for the development of methods to cool and trap atoms with laser light.

2 Cornell, E.A., Ketterle, W. and Weiman, C.E. (**2001**) Nobel Prize in Physics for the achievement of Bose–Einstein condensation in dilute gases of alkali atoms, and for early fundamental studies of the properties of the condensates.

3 Pringsheim, P. (**1929**) Zwei Bemerkungen über den Unterchied von Luminneszenz- und Temperaturstrahlung, *Z. Phys.*, **57**, 739.

4 Edwards, B.C., Buchwald, M.I. and Epstein, R.I. (**1998**) Development of the Los-Alamos Solid-State Optical Refrigerator, *Rev. Sci. Instrum.*, **69**, 2050–2055.

5 Edwards, B.C., Anderson, J.E., Epstein, R.I., Mills, G.L. and Mord, A.J. (**1999**) Demonstration of a solid-state optical cooler: An approach to cryogenic refrigeration, *J. Appl. Phys.*, **86**, 6489–6493.

6 Sheik-Bahae, M. and Epstein, R.I. (**2007**) Optical refrigeration, *Nature Photonics*, **1**, 693–699.

7 Mills, G. and Mord, A. (**2005**) Performance modeling of optical refrigerators, *Cryogenics*, **46**, 176–182.

8 Bowman, S.R. (**1999**) Lasers without internal heat generation, *IEEE J. Quant. Elect.*, **35**, 115–122.

9 Bowman, S.R. and Mungan, C.E. (**2000**) New materials for optical cooling, *Applied Physics B*, **71**, 807–811.

10 Landau, L. (**1946**) On the thermondynamics of photoluminescence, *J. Phys.* (Moscow), **10**, 503.

11 Kastler, A. (**1950**) Quelques suggestions concernant la production optique et la détection optique d'une inégalité de population des niveaux de quantification spatiale des atomes application a l'expérience de Stern et Gerlach et a la résonance magnétique, *J. Phys. Radium*, **11**, 255–265.

12 Kushida, T. and Geusic, J.E. (**1968**) Optical refrigeration in Nd-doped yttrium aluminum garnet, *Phys. Rev. Lett.*, **21**, 1172–1175.

13 Yatsiv, S. (**1961**) Anti-Stokes fluorescence as a cooling process, in *Advances in Quantum Electronics*, (ed J.R. Singer), New York, Columbia Univ., 200–213.

14 Epstein, R.I., Buchwald, M.I., Edwards, B.C., Gosnell, T.R. and Mungan, C.E. (**1995**) Observation of laser-induced fluorescent cooling of a solid, *Nature*, **377**, 500–503.

15 Sheik-Bahae, M. and Epstein, R.I. (**2004**) Can laser light cool Semiconductors?, *Phys. Rev. Lett.*, **92**, 247403.

16 Asbeck, P. (**1977**) Self-absorption effects on radiative lifetime in GaAs–GaAlAs Double Heterostructures, *J. Appl. Phys.*, **48**, 820-822.

17 Sheik-Bahae, M., Imangholi, B., Hasselbeck, M.P., Epstein, R.I. and Kurtz, S. (**2006**) Advances in laser cooling of semiconductors, in *Proceedings of SPIE: Physics and Simulation of Optoelectronic Devices XIV*, vol. 6115, (eds M. Osinski, F. Henneberger and Y. Arakawa), Bellingham, SPIE, pp. 611518.

18 Emin, D. (**2007**) Laser cooling via excitation of localized electrons, *Phys. Rev. B*, 76, 024301.

19 Mungan, C.E., Buchwald, M.I., Edwards, B.C., Epstein, R.I. and Gosnell, T.R. (**1997**) Laser cooling of a solid by 16 K starting from room-temperature, *Phys. Rev. Lett.*, **78**, 1030–1033.

20 Luo, X., Eisaman, M.D. and Gosnell, T.R. (**1998**) Laser cooling of a solid by 21 K starting from room temperature, *Opt. Lett.*, **23**, 639–641.

21 Gosnell, T.R. (**1999**) Laser cooling of a solid by 65 K starting from room temperature, *Opt. Lett.*, **24**, 1041–1043.

22 Thiede, J., Distel, J., Greenfield, S.R. and Epstein, R.I. (**2005**) Cooling to 208 K by optical refrigeration, *Appl. Phys. Lett.*, **86**, 154107.

23 Rayner, A., Friese, M.E.J., Truscott, A.G., Heckenberg, N.R. and Rubinsztein-Dunlop, H. (**2001**) Laser cooling of a solid from ambient temperature, *J. Mod. Opt.*, **48**, 103–114.

24 Heeg, B., Stone, M.D., Khizhnyak, A., Rumbles, G., Mills, G. and DeBarber, P.A. (**2004**) Experimental demonstration of intracavity solid-state laser cooling of Yb^{3+}: ZrF_4–BaF_2–LaF_3–AlF_3–NaF glass, *Phys. Rev. A*, **70**, 021401.

25 Fernandez, J.R., Mendioroz, A., Balda, R., Voda, M., Al-Saleh, M., Garcia-Adeva, A.J., Adam, J.-L. and Lucas, J. (**2002**) Origin of laser-induced internal cooling of Yb^{3+}-doped systems, Rare-Earth-Doped Materials and Devices VI, vol. 4645, S. Jiang and R.W. Keys, Eds., Bellingham, SPIE, pp. 135–147.

26 Fernandez, J., Mendioroz, A., Garcia, A.J., Balda, R. and Adam, J.L. (**2000**) Anti-Stokes laser-induced internal cooling of Yb^{3+}-doped glasses, *Phys. Rev. B*, **62**, 3213–3217.

27 Epstein, R.I., Brown, J.J., Edwards, B.C. and Gibbs, A. (**2001**) Measurements of optical refrigeration in ytterbium-doped crystals, *J. Appl. Phys.*, **90**, 4815–4819.

28 Mendioroz, A., Fernandez, J., Voda, M., Al-Saleh, M., Balda, R. and Garcia-Adeva, A. (**2002**) Anti-stokes laser cooling in Yb^{3+}-doped KPb_2Cl_5 crystal, *Opt. Lett.*, **27**, 1525–1527.

29 Bigotta, S., Parisi, D., Bonelli, L., Toncelli, A., Di Lieto, A. and Tonelli, M. (**2006**) Laser cooling of Yb^{3+}-doped BaY_2F_8 single crystal, *Opt. Mater.*, **28**, 1321–1324.

30 Bigotta, S., Parisi, D., Bonelli, L., Toncelli, A., Tonelli, M. and Di Lieto, A. (**2006**) Spectroscopic and laser cooling results on Yb^{3+}-doped BaY_2F_8 single crystal, *J. Appl. Phys.*, **100**, 013109.

31 Patterson, W., Bigotta, S., Sheik-Bahae, M., Parisi, D., Tonelli, M. and Epstein, R. (**2008**) Anti-Stokes luminescence cooling of Tm^{3+}-doped BaY_2F_8, *Opt. Express*, **16**, 1704–1710.

32 Bigotta, S., Lieto, A.D., Parisi, D., Toncelli, A. and Tonelli, M. (**2007**) *Single fluoride crystals as materials for laser cooling applications*, presented at Laser Cooling of Solids, San Jose, CA, USA, 24–25 Jan.

33 Seletskiy, D., Hasselbeck, M.P., Sheik-Bahae, M., Epstein, R.I. Bigotta, S. and Tonelli, M. (**2008**) Cooling of Yb:YLF using cavity enhanced resonant absorption, presented at Laser Refrigeration of Solids, San Jose, CA, USA, 23–24 Jan.

34 Hoyt, C.W., Sheik-Bahae, M., Epstein, R.I., Edwards, B.C. and Anderson, J.E. (**2000**) Observation of anti-Stokes fluorescence cooling in thulium-doped glass, *Phys. Rev. Lett.*, **85**, 3600–3603.

35 Hoyt, C., Hasselbeck, M., Sheik-Bahae, M., Epstein, R., Greenfield, S., Thiede, J., Distel, J. and Valencia, J. (**2003**) Ad-

vances in laser cooling of thulium-doped glass, *J. Opt. Soc. Am. B*, **20**, 1066–1074.

36 Fernandez, J., Garcia-Adeva, A.J. and Balda, R. (**2006**) Anti-Stokes laser cooling in bulk erbium-doped materials, *Phys. Rev. Lett.*, **97**, 033001.

37 Garcia-Adeva, A.J., Balda, R. and Fernandez, J. (**2007**) Anti-Stokes laser cooling in erbium-doped low-phonon materials, in *Laser Cooling of Solids*, vol. 6461, (eds R.I. Epstein and M. Sheik-Bahae), Bellingham, SPIE, pp. 646102-1.

38 Lamouche, G., Lavallard, P., Suris, R. and Grousson, R. (**1998**) Low temperature laser cooling with a rare-earth doped glass, *J. Appl. Phys.*, **84**, 509–516.

39 Hehlen, M.P., Epstein, R.I. and Inoue, H. (**2007**) Model of laser cooling in the Yb^{3+}-doped fluorozirconate glass ZBLAN, *Phys. Rev. B*, **75**, 144302.

40 Hoyt, C.W. (**2003**) Laser Cooling in Thulium-Doped Solids, Ph.D. Thesis, University of New Mexico, 138 pp.

41 Seletskiy, D., Hasselbeck, M.P., Sheik-Bahae, M. and Epstein, R.I. (**2007**) Laser cooling using cavity enhanced pump absorption, in *Proceeding of SPIE: Laser Cooling of Solids*, vol. 6461, (eds R.I. Epstein and M. Sheik-Bahae), Bellingham, SPIE, 646104.

42 Ruan, X.L. and Kaviany, M. (**2006**) Enhanced laser cooling of rare-earth-ion-doped nanocrystalline powders, *Phys. Rev. B*, **73**, 155422.

43 Clark, J.L. and Rumbles, G. (**1996**) Laser cooling in the condensed-phase by frequency up-conversion, *Phys. Rev. Lett.*, **76**, 2037–2040.

44 Oraevsky, A.N. (**1996**) Cooling of semiconductors by laser radiation, *J. Russ. Laser Res.*, **17**, 471–479.

45 Rivlin, L.A. and Zadernovsky, A.A. (**1997**) Laser cooling of semiconductors, *Opt. Commun.*, **139**, 219–222.

46 Gauck, H., Gfroerer, T.H., Renn, M.J., Cornell, E.A. and Bertness, K.A. (**1997**) External radiative quantum efficiency of 96% from a GaAs/GaInP heterostructure, *Appl. Phys. A*, **64**, 143–147.

47 Rupper, G., Kwong, N.H. and Binder, R. (**2006**) Large excitonic enhancement of optical refrigeration in semiconductors, *Phys. Rev. Lett.*, **97**, 117401.

48 Huang, D.H., Apostolova, T., Alsing, P.M. and Cardimona, D.A. (**2005**) Spatially selective laser cooling of carriers in semiconductor quantum wells, *Phys. Rev. B*, **72**, 195308.

49 Li, J.Z. (**2007**) Laser cooling of semiconductor quantum wells: Theoretical framework and strategy for deep optical refrigeration by luminescence upconversion, *Phys. Rev. B*, **75**, 155315.

50 Rupper, G., Kwong, N.H. and Binder, R. (**2007**) Optical refrigeration of GaAs: Theoretical study, *Phys. Rev. B*, **76**, 245203.

51 Huang, D. and Alsing, P.M. (**2008**) Many-body effects on optical carrier cooling in intrinsic semiconductors at low lattice temperatures, *Phys. Rev. B*, **78**, 035206.

52 Khurgin, J.B. (**2008**) Role of bandtail states in laser cooling of semiconductors, *Phys. Rev. B*, **77**, 235206.

53 Finkeissen, E., Potemski, M., Wyder, P., Vina, L. and Weimann, G. (**1999**) Cooling of a semiconductor by luminescence up-conversion, *Appl. Phys. Lett.*, **75**, 1258–1260.

54 Gfroerer, T.H., Cornell, E.A. and Wanlass, M.W. (**1998**) Efficient directional spontaneous emission from an InGaAs/InP heterostructure with an integral parabolic reflector, *J. Appl. Phys.*, **84**, 5360–5362.

55 Imangholi, B., Hasselbeck, M.P., Sheik-Bahae, M., Epstein, R.I. and Kurtz, S. (**2005**) Effects of epitaxial lift-off on interface recombination and laser cooling in GaInP/GaAs heterostructures, *Appl. Phys. Lett.*, **86**, 81104.

56 Eshlaghi, S., Worthoff, W., Wieck, A.D. and Suter, D. (**2008**) Luminescence upconversion in GaAs quantum wells, *Phys. Rev. B*, **77**, 245317.

57 Khurgin, J.B. (**2007**) Surface plasmon-assisted laser cooling of solids, *Phys. Rev. Lett.*, **98**, 177401.

58 Khurgin, J.B. (**2006**) Band gap engineering for laser cooling of semiconductors, *J. Appl. Phys.*, **100**, 113116.

59 Basu, P.K. (**1997**) Theory of Optical Processes in Semiconductors: Bulk and Microstructures, New York: Oxford Univ. Press.

60 Pankove, J.I. (**1971**) Optical Processes in Semiconductors, Englewood Cliffs, Prentice-Hall.

61 Born, M. and Wolf, E. (**1999**) Principles of Optics: Electromagnetic Theory of Propagation, Interference and Diffraction of Light, 7th expanded ed., Cambridge, Cambridge Univ. Press.

62 van Roosbroeck, W. and Shockley, W. (**1954**) *Phys. Rev.*, **94**, 1558.

63 Chuang, S.L. (**1995**) Physics of Optoelectronic Devices, New York, John Wiley & Sons, Inc.

64 Piprek, J. (**2003**) Semiconductor Optoelectronic Devices: Introduction to Physics and Simulation, Amsterdam, Academic.

65 Yablonovitch, E., Gmitter, T.J. and Bhat, R. (**1988**) Inhibited and enhanced spontaneous emission from optically thin AlGaAs/GaAs double heterostructures, *Phys. Rev. Lett.*, **61**, 2546–2549.

66 Haug, A. (**1992**) Free-carrier absorption in semiconductor-lasers, *Semicond. Sci. Tech.*, **7**, 373–378.

67 Yi, H., Diaz, J., Lane, B. and Razeghi, M. (**1996**) Optical losses of Al-free lasers for λ = 0.808 and 0.98 μm, *Appl. Phys. Lett.*, **69**, 2983–2985.

68 Imangholi, B. (**2006**) Investigation of laser cooling in semiconductors, Ph.D. Thesis, University of New Mexico, 210 pp.

69 Agrawal, G.P. and Dutta, N.K. (**1986**) Long-wavelength semiconductor lasers, New York, Van Nostrand Reinhold.

70 Thooft, G.W. and Vanopdorp, C. (**1983**) Temperature-dependence of interface recombination and radiative recombination in (AL,GA)AS heterostructures, *Appl. Phys. Lett.*, **42**, 813–815.

71 Ahrenkiel, R.K., Olson, J.M., Dunlavy, D.J., Keyes, B.M. and Kibbler, A.E. (**1990**) Recombination velocity of the $Ga_{0.5}In_{0.5}P$/GaAs interface, *J. Vac. Sci. Technol. A*, **8**, 3002–3005.

72 Olson, J.M., Ahrenkiel, R.K., Dunlavy, D.J., Keyes, B. and Kibbler, A.E. (**1989**) Ultralow recombination velocity at $Ga_{0.5}In_{0.5}P$/GaAs heterointerfaces, *Appl. Phys. Lett.*, **55**, 1208–1210.

73 Schaefer, A.C. and Steel, D.G. (**1997**) Nonlinear optical response of the GaAs exciton polariton, *Phys. Rev. Lett.*, **79**, 4870–4873.

74 Butov, L.V., Lai, C.W., Ivanov, A.L., Gossard, A.C. and Chemla, D.S. (**2002**) Towards Bose–Einstein condensation of excitons in potential traps, *Nature*, **417**, 47–52.

75 Banyai, L. and Koch, S.W. (**1986**) A simple theory for the effects of plasma screening on the optical-spectra of highly excited semiconductors, *Z. Phys. B*, **63**, 283–291.

76 Haug, H. and Koch, S.W. (**1994**) Quantum Theory of the Optical and Electronic Properties of Semiconductors, 3rd edn, Singapore: World Scientific.

77 Lowenau, J.P., Reich, F.M. and Gornik, E. (**1995**) Many-body theory of room-temperature optical nonlinearities in bulk semiconductors, *Phys. Rev. B*, **51**, 4159–4165.

78 Meier, T. and Koch, S.W. (**2001**) Coulomb correlation signatures in the excitonic optical nonlinearities of semiconductors, *Semicond. Semimet.*, **67**, 231–313.

79 Rupper, G., Kwong, N.H. and Binder, R. (**2007**) Optical refrigeration of GaAs: Theoretical study, *Phys. Rev. B*, **76**, 245203.

80 Hasselbeck, M.P., Sheik-Bahae, M. and Epstein, R.I. (**2007**) Effect of high carrier density on luminescence thermometry in semiconductors, in *Proceedings of SPIE: Laser Cooling of Solids*, vol. 6461, (eds R.I. Epstein and M. Sheik-Bahae), Bellingham, SPIE, 646107.

81 Imangholi, B., Hasselbeck, M.P. and Sheik-Bahae, M. (**2003**) Absorption spectra of wide-gap semiconductors in their transparency region, *Opt. Commun.*, **227**, 337–341.

82 Catchpole, K.R., Lin, K.L., Campbell, P., Green, M.A., Bett, A.W. and Dimroth, F. (**2004**) High external quantum efficiency of planar semiconductor structures, *Semicond. Sci. Tech.*, **19**, 1232–1235.

83 Martin, R.P., Velten, J., Stintz, A., Malloy, K.J., Epstein, R.I., Sheik-Bahae, M., Hasselbeck, M.P., Imangholi, B., Boyd, S.T.P. and Bauer, T.M. (**2007**) Nanogap experiments for laser cooling: a progress report, in *Proceedings of SPIE: Laser Cooling of Solids*, vol. 6461, (eds R.I. Epstein

and M. Sheik-Bahae), Bellingham, SPIE, 64610H.

84 Epstein, R.I., Edwards, B.C. and Sheik-Bahae, M. (**2002**) Semiconductor-Based Optical Refrigerator, US Patent 6 378 321.

85 Edwards, B.C., Buchwald, M.I. and Epstein, R.I. (**2000**) Optical refrigerator using reflectivity tuned dielectric mirrors, US Patent 6 041 610.